Measurement of the Time-Dependent CP Asymmetries in $B^0 \to K^0_S \rho^0 \gamma$ Decays

J. Li,[6] I. Adachi,[7] K. Arinstein,[1] T. Aushev,[17,12] A. M. Bakich,[37] V. Balagura,[12] I. Bedny,[1] V. Bhardwaj,[32] U. Bitenc,[13] A. Bozek,[26] M. Bračko,[19,13] T. E. Browder,[6] P. Chang,[25] Y. Chao,[25] A. Chen,[23] B. G. Cheon,[5] R. Chistov,[12] Y. Choi,[36] J. Dalseno,[7] A. Drutskoy,[3] S. Eidelman,[1] N. Gabyshev,[1] H. Ha,[15] K. Hara,[21] Y. Hasegawa,[35] H. Hayashii,[22] M. Hazumi,[7] D. Heffernan,[31] Y. Hoshi,[40] W.-S. Hou,[25] H. J. Hyun,[16] T. Iijima,[21] A. Ishikawa,[33] R. Itoh,[7] M. Iwasaki,[42] Y. Iwasaki,[7] N. J. Joshi,[38] D. H. Kah,[16] J. H. Kang,[46] H. Kawai,[2] T. Kawasaki,[28] H. Kichimi,[7] Y. I. Kim,[16] Y. J. Kim,[4] K. Kinoshita,[3] S. Korpar,[19,13] P. Križan,[18,13] P. Krokovny,[7] R. Kumar,[32] A. Kuzmin,[1] S.-H. Kyeong,[46] C. Liu,[34] Y. Liu,[4] A. Matyja,[26] S. McOnie,[37] T. Medvedeva,[12] K. Miyabayashi,[22] H. Miyake,[31] H. Miyata,[28] G. R. Moloney,[20] Y. Nagasaka,[8] M. Nakao,[7] Z. Natkaniec,[26] S. Nishida,[7] O. Nitoh,[44] S. Ogawa,[39] T. Ohshima,[21] S. Okuno,[14] S. L. Olsen,[6,9] H. Ozaki,[7] G. Pakhlova,[12] C. W. Park,[36] H. Park,[16] H. K. Park,[16] K. S. Park,[36] L. S. Peak,[37] R. Pestotnik,[13] L. E. Piilonen,[45] H. Sahoo,[6] Y. Sakai,[7] O. Schneider,[17] C. Schwanda,[10] A. Sekiya,[22] K. Senyo,[21] M. Shapkin,[11] J.-G. Shiu,[25] B. Shwartz,[1] A. Sokolov,[11] A. Somov,[3] S. Stanič,[29] M. Starič,[13] T. Sumiyoshi,[43] M. Tanaka,[7] G. N. Taylor,[20] Y. Teramoto,[30] I. Tikhomirov,[12] K. Trabelsi,[7] T. Tsuboyama,[7] S. Uehara,[7] T. Uglov,[12] Y. Unno,[5] S. Uno,[7] P. Urquijo,[20] Y. Ushiroda,[7] Y. Usov,[1] G. Varner,[6] K. E. Varvell,[37] K. Vervink,[17] A. Vinokurova,[1] C. H. Wang,[24] P. Wang,[9] X. L. Wang,[9] Y. Watanabe,[14] E. Won,[15] B. D. Yabsley,[37] H. Yamamoto,[41] Y. Yamashita,[27] M. Yamauchi,[7] Z. P. Zhang,[34] V. Zhilich,[1] T. Zivko,[13] A. Zupanc,[13] and O. Zyukova[1]

(Belle Collaboration)

[1]*Budker Institute of Nuclear Physics, Novosibirsk*
[2]*Chiba University, Chiba*
[3]*University of Cincinnati, Cincinnati, Ohio 45221*
[4]*The Graduate University for Advanced Studies, Hayama*
[5]*Hanyang University, Seoul*
[6]*University of Hawaii, Honolulu, Hawaii 96822*
[7]*High Energy Accelerator Research Organization (KEK), Tsukuba*
[8]*Hiroshima Institute of Technology, Hiroshima*
[9]*Institute of High Energy Physics, Chinese Academy of Sciences, Beijing*
[10]*Institute of High Energy Physics, Vienna*
[11]*Institute of High Energy Physics, Protvino*
[12]*Institute for Theoretical and Experimental Physics, Moscow*
[13]*J. Stefan Institute, Ljubljana*
[14]*Kanagawa University, Yokohama*
[15]*Korea University, Seoul*
[16]*Kyungpook National University, Taegu*
[17]*École Polytechnique Fédérale de Lausanne (EPFL), Lausanne*
[18]*Faculty of Mathematics and Physics, University of Ljubljana, Ljubljana*
[19]*University of Maribor, Maribor*
[20]*University of Melbourne, School of Physics, Victoria 3010*
[21]*Nagoya University, Nagoya*
[22]*Nara Women's University, Nara*
[23]*National Central University, Chung-li*
[24]*National United University, Miao Li*
[25]*Department of Physics, National Taiwan University, Taipei*
[26]*H. Niewodniczanski Institute of Nuclear Physics, Krakow*
[27]*Nippon Dental University, Niigata*
[28]*Niigata University, Niigata*
[29]*University of Nova Gorica, Nova Gorica*
[30]*Osaka City University, Osaka*
[31]*Osaka University, Osaka*
[32]*Panjab University, Chandigarh*
[33]*Saga University, Saga*
[34]*University of Science and Technology of China, Hefei*
[35]*Shinshu University, Nagano*
[36]*Sungkyunkwan University, Suwon*

[37]University of Sydney, Sydney, New South Wales
[38]Tata Institute of Fundamental Research, Mumbai
[39]Toho University, Funabashi
[40]Tohoku Gakuin University, Tagajo
[41]Tohoku University, Sendai
[42]Department of Physics, University of Tokyo, Tokyo
[43]Tokyo Metropolitan University, Tokyo
[44]Tokyo University of Agriculture and Technology, Tokyo
[45]Virginia Polytechnic Institute and State University, Blacksburg, Virginia 24061
[46]Yonsei University, Seoul

(Received 16 June 2008; published 15 December 2008)

We report the first measurement of time-dependent CP asymmetry in $B^0 \to K^0_S \rho^0 \gamma$ decays based on 657×10^6 $B\bar{B}$ pairs collected with the Belle detector at the KEKB asymmetric-energy collider. We measure the CP-violating parameter $\mathcal{S}_{K^0_S\rho^0\gamma} = 0.11 \pm 0.33(\text{stat})^{+0.05}_{-0.09}(\text{syst})$ from a signal of 212 ± 17 events. We also obtain the effective direct CP-violating parameter $\mathcal{A}_{\text{eff}} = 0.05 \pm 0.18(\text{stat}) \pm 0.06(\text{syst})$ for $m_{K^0_S\pi^+\pi^-} < 1.8$ GeV/c^2 and 0.6 GeV/$c^2 < m_{\pi^+\pi^-} < 0.9$ GeV/c^2.

DOI: 10.1103/PhysRevLett.101.251601 PACS numbers: 11.30.Er, 13.20.He

In the standard model (SM), a mostly left- (right-) handed photon emitted from a $\bar{B}^0$ (B^0) meson is expected in the $b \to s\gamma$ transition. Hence a small time-dependent CP asymmetry is predicted in decays of the type $B \to f_{CP}\gamma$ [1], where f_{CP} is a CP eigenstate. New physics may lead to deviations from the SM expectation by introducing different photon polarizations in the transition, and can be probed via experimental measurements of CP asymmetries [2]. In multibody final states $B^0 \to P^0 Q^0 \gamma$ with P^0 and Q^0 being C eigenstates, the same argument holds [3]. Measurements of the time-dependent CP asymmetry in $B^0 \to K^0_S \pi^0 \gamma$ have been reported by Belle and *BABAR* based on 535×10^6 and 431×10^6 $B\bar{B}$ pairs [4,5], respectively. In this Letter, using 657×10^6 $B\bar{B}$ pairs collected with the Belle detector [6] at the KEKB asymmetric-energy e^+e^- collider [7], we report the measurement of CP-violating parameters in a new channel $B^0 \to K^0_S \rho^0 \gamma$ where the B^0 decay vertex can be reconstructed from the two charged pions in the ρ^0 decay. In this case $C(K^0_S)C(\rho^0) = +1$, and the SM predicts a small asymmetry $\mathcal{S}_{K^0_S\rho^0\gamma} \approx 0.03$ [3].

At the KEKB, the $\Upsilon(4S)$ is produced with a Lorentz boost of $\beta\gamma = 0.425$ along the z axis, which is defined as the direction antiparallel to the e^+ beam direction. In the decay chain $\Upsilon(4S) \to B^0\bar{B}^0 \to f_{\text{sig}} f_{\text{tag}}$, where one of the B mesons decays at time t_{sig} to the signal mode f_{sig} and the other decays at time t_{tag} to a final state f_{tag} that distinguishes B^0 and $\bar{B}^0$, the time-dependent decay rate is given by

$$P(\Delta t, q) = \frac{e^{-|\Delta t|/\tau_{B^0}}}{4\tau_{B^0}}\{1 + q[\mathcal{S}\sin(\Delta m_d \Delta t) + \mathcal{A}\cos(\Delta m_d \Delta t)]\}. \quad (1)$$

Here the probability density function (PDF) is normalized as a function of two variables: B flavor $q = +1(-1)$ when the tagging B meson is $B^0(\bar{B}^0)$, and decay time difference Δt between two B mesons. In Eq. (1), $\mathcal{S}$ and $\mathcal{A}$ are CP-violating parameters, τ_{B^0} is the B^0 lifetime, Δm_d is the mass difference between the two B^0 mass eigenstates. Since the $B^0\bar{B}^0$ mesons are approximately at rest in the $\Upsilon(4S)$ center-of-mass system (c.m.s.), Δt can be determined from Δz, the displacement in z between the f_{sig} and f_{tag} decay vertices: $\Delta t \simeq \Delta z/(\beta\gamma c)$.

The Belle detector [6] is a large solid-angle magnetic spectrometer that consists of a silicon vertex detector, a 50-layer central drift chamber, an array of aerogel threshold Cherenkov counters, an electromagnetic calorimeter (ECL) composed of CsI(Tl) crystals and a K^0_L-muon detector.

High energy photons are selected from isolated ECL clusters with no corresponding charged track and c.m.s. energy satisfying $1.4 < E^*_\gamma < 3.4$ GeV. The photons are required to lie in the barrel region of the ECL, and have a photon showerlike shape $E_9/E_{25} > 0.95$, where E_9 and E_{25} are the energies summed in 3×3 and 5×5 arrays of crystals around the center of the shower, respectively. To reduce background from $\pi^0 \to \gamma\gamma$ or $\eta \to \gamma\gamma$, a $\pi^0(\eta)$ veto is applied with $\mathcal{L}_{\pi^0} < 0.25$ ($\mathcal{L}_\eta < 0.2$), where $\mathcal{L}_{\pi^0(\eta)}$ is a $\pi^0(\eta)$ likelihood described in Ref. [8].

Neutral kaons (K^0_S) are reconstructed from two oppositely charged pions whose invariant mass lies within 15 MeV/c^2 of the K^0_S nominal mass. Requirements on impact parameter and vertex displacement are applied [9].

Charged tracks are required to originate from the vicinity of the interaction point. Charged pions should have kaon and pion identification likelihoods consistent with the pion hypothesis. This requirement has an efficiency of 85% with a 7% kaon fake rate.

The decay $B^+ \to K^+\pi^-\pi^+\gamma$ is also reconstructed to study the $K\pi\pi$ system and to serve as a control sample. Charged kaons are selected from charged tracks and required to be identified as kaons with 86% efficiency and an 8% pion fake rate.

We form two kinematic variables: the energy difference $\Delta E = E_B^* - E_{\rm beam}^*$ and the beam-energy constrained mass $M_{\rm bc} = \sqrt{(E_{\rm beam}^*)^2 - (p_B^*)^2}$, where $E_{\rm beam}^*$ is the beam energy in the c.m.s., and E_B^* and p_B^* are the c.m.s. energy and momentum of the reconstructed B candidate, respectively. The requirement $-0.1 < \Delta E < 0.08$ GeV is applied. The $K^+\pi^-\pi^+$ and $K_S^0\pi^-\pi^+$ invariant masses are required to be less than 1.8 GeV/c^2.

The $B^0 \to K_S^0\rho^0\gamma$ candidates are selected from the $K_S^0\pi^+\pi^-\gamma$ sample by requiring the $\pi^+\pi^-$ invariant mass to lie in the ρ^0 region, $0.6 < m_{\pi\pi} < 0.9$ GeV/c^2. Since the ρ^0 is wide, other modes, such as $K^{*+}\pi^-\gamma$, may also contribute. We first measure the effective CP-violating parameters, $\mathcal{S}_{\rm eff}$ and $\mathcal{A}_{\rm eff}$, using the final sample and then convert $\mathcal{S}_{\rm eff}$ to $\mathcal{S}_{K_S^0\rho^0\gamma}$ for $B^0 \to K_S^0\rho^0\gamma$ using a dilution factor $\mathcal{D}$, which is discussed later.

In order to suppress the background from light quark pair production $q\bar{q}$ ($e^+e^- \to q\bar{q}$ with $q = u, d, s, c$), a selection based on an event likelihood ratio $\mathcal{R} \equiv \mathcal{L}_{\rm sig}/(\mathcal{L}_{\rm sig} + \mathcal{L}_{\rm bkg})$ is applied. The $\mathcal{R}$ selection was optimized using a figure-of-merit study and has a signal efficiency of 52.0%, while rejecting 95.5% of the $q\bar{q}$ background. The likelihood for signal ($\mathcal{L}_{\rm sig}$) and background ($\mathcal{L}_{\rm bkg}$) is formed by combining a Fisher discriminant $\mathcal{F}$ that uses extended modified Fox-Wolfram moments [10] and the polar angle of the B meson in the c.m.s. ($\cos\theta_B$). There are multiple candidates in 18.4% of all the events; we choose the candidate that has the largest $\mathcal{R}$. We define ΔE sideband events with the criterion $0.1 < \Delta E < 0.5$ GeV and by vetoing $B \to (K\pi^\pm)\gamma$. Other backgrounds that pass our selection criteria are classified as (a) $B \to K^*\gamma$ background, (b) $B \to X_s\gamma$ background, or (c) $B\bar{B}$ background, which includes a generic $b \to c$ component and charmless B-decay component.

The self-cross-feed (SCF) component consists of events in which not all tracks are from the signal side, in contrast to a true signal with all tracks correctly assigned. We define the total signal yield as the sum of SCF and true signal events. The fraction of SCF in the total signal yield ranges from 5.5% to 10.8% in the $M_{\rm bc}$ signal region defined as $5.27 < M_{\rm bc} < 5.29$ GeV/c^2, depending on the kaonic resonance.

We obtain the flavor q, tagging quality factor $r \in [0, 1]$, and signal and tag side vertices from the procedure described in Ref. [11], using the two charged π's to reconstruct the signal vertex. There is no flavor discrimination when $r = 0$, while the flavor tagging is unambiguous when $r = 1$. Events are sorted into seven r bins.

We obtain 299 events in the signal $M_{\rm bc}$ region after vertexing. An unbinned maximum likelihood fit to $M_{\rm bc}$ is applied with signal and $q\bar{q}$ yields floated in each r bin. In the signal $M_{\rm bc}$ region, we find 212 ± 17 total signal with 6.0% SCF, 53.4 ± 2.6 $q\bar{q}$, along with 7.8 $K^*\gamma$, 21.5 other $X_s\gamma$, and 9.0 $B\bar{B}$ events. We obtain the branching fraction $\mathcal{B}(B^0 \to K^0\pi^+\pi^-) = [1.87 \pm 0.13(\text{stat})] \times 10^{-5}$, for $m(K^0\pi\pi) < 1.8$ GeV/c^2, which is consistent with other recent measurements [12]. The true signal shape is parametrized as a crystal ball function [13] with a width corrected using the $B^+ \to K^+\pi^-\pi^+\gamma$ data. The $q\bar{q}$ shape is obtained from the ΔE sideband events. For other backgrounds and SCFs, shapes and r-dependent fractions are obtained from Monte Carlo (MC) calculations since their contributions are small. Figure 1 shows the $M_{\rm bc}$ projection of the fit.

The $\mathcal{S}_{\rm eff}$ and $\mathcal{A}_{\rm eff}$ parameters are extracted from an unbinned maximum likelihood fit to the Δt distribution, shown in Fig. 2. The likelihood function for event i is

$$P_i = (1 - f_{\rm ol}) \int_{-\infty}^{+\infty} d(\Delta t') \Big[\sum_j f_j P_j(\Delta t') R_j(\Delta t_i - \Delta t') \Big] + f_{\rm ol} P_{\rm ol}(\Delta t_i), \quad (2)$$

where j runs over the signal, SCF, and four background (BG) components ($q\bar{q}$, $K^*\gamma$, other $X_s\gamma$, $B\bar{B}$). The fraction of each component (f_j) is calculated using the r dependent $M_{\rm bc}$ fit result on an event-by-event basis. R_j is the Δt resolution function. $P_{\rm ol}$ is a Gaussian function that represents a small outlier component with fraction $f_{\rm ol}$.

The PDF for the signal Δt distribution $P_{\rm sig}$ is given by a modified form of Eq. (1), which incorporates the effect of incorrect flavor assignment. The parametrization of R is the same as the one used in the $B^0 \to \phi K^0$ analysis [9]. The PDF for SCF ($P_{\rm SCF}$) is the same as for the signal but uses a shorter lifetime 1.16 ± 0.02 ps, determined from a MC study. The same functional forms for the PDF and resolution are used for the $K^*\gamma$, other $X_s\gamma$ and $B\bar{B}$ components but with lifetime values obtained from MC calculations and CP parameters fixed to zero. The PDF for $q\bar{q}$ background events, $P_{q\bar{q}}$, is modeled as a δ function convolved with a double-Gaussian resolution function $R_{q\bar{q}}$.

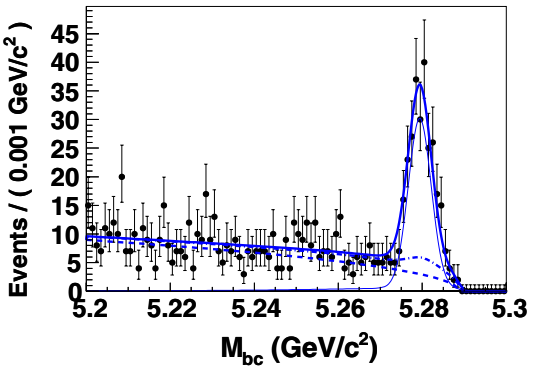

FIG. 1 (color online). $M_{\rm bc}$ distributions for $B^0 \to K_S^0\pi^+\pi^-\gamma$ events. Points with error bars are data. The curves show the results from the r dependent $M_{\rm bc}$ fit. The dashed curve and the dash-dotted curve correspond to $q\bar{q}$ and the sum of all BGs. The thin curve is the total signal including SCF and the thick curve is the total PDF.

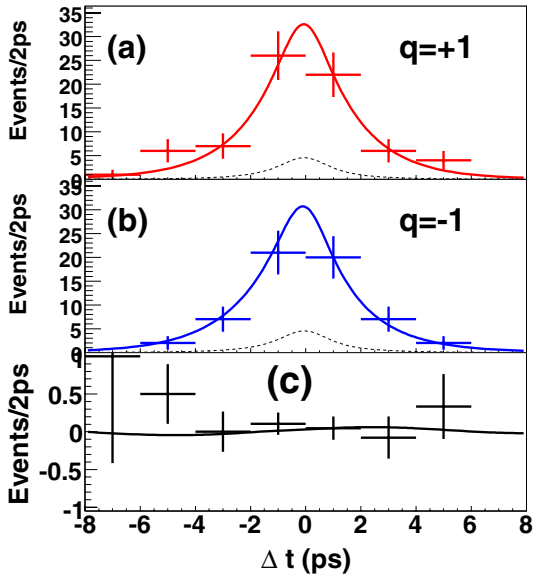

FIG. 2 (color online). (a) $q = +1$ yield, (b) $q = -1$ yield, and (c) raw asymmetry as a function of Δt for events with $r > 0.5$. The raw asymmetry is defined as $(N_+ - N_-)/(N_+ + N_-)$ where N_+ (N_-) is the event yield with $q = +1(-1)$. The solid curves are the fits while the dashed curves show the background contributions.

The parameters in $R_{q\bar{q}}$ are determined from a fit to ΔE sideband events.

The only free parameters in the CP fit to $B^0 \to K^0_S\pi^+\pi^-\gamma$ are $\mathcal{S}_{\rm eff}$ and $\mathcal{A}_{\rm eff}$, which are determined by maximizing the likelihood function $L = \prod_i P_i$ for events in the $M_{\rm bc}$ signal region. We obtain $\mathcal{S}_{\rm eff} = 0.09 \pm 0.27({\rm stat})^{+0.04}_{-0.07}({\rm syst})$ and $\mathcal{A}_{\rm eff} = 0.05 \pm 0.18({\rm stat}) \pm 0.06({\rm syst})$.

The lifetime fit gives 1.575 ± 0.066 ps for $B^+ \to K^+\pi^-\pi^+\gamma$ and 1.50 ± 0.15 ps for $B^0 \to K^0_S\pi^+\pi^-\gamma$, which are consistent with the nominal B^+ and B^0 lifetimes [12]. A CP fit for the control sample $B^+ \to K^+\pi^-\pi^+\gamma$ gives CP parameters $S = 0.17 \pm 0.11$ and $A = -0.13 \pm 0.08$, which are consistent with zero.

We evaluate systematic uncertainties from the following sources. The largest contribution is due to the vertex reconstruction, where the selection criteria are varied to determine the systematics, which gives $\Delta\mathcal{S}_{\rm eff} = {}^{+0.01}_{-0.06}$, $\Delta\mathcal{A}_{\rm eff} = \pm 0.03$. The $\mathcal{S}$ values for $b \to s$ CP modes are varied from 0 to $\sin 2\phi_1$ to estimate the effect of CP asymmetry in the $B\bar{B}$ background. We fit the data with each fixed parameter shifted by its error to evaluate the uncertainties due to background and SCF fractions, shapes, Δt PDFs, resolution function, flavor tagging, and physics parameters τ_{B^0}, Δm_d. Effects of tag side interference are evaluated in the same way as in Ref. [4].

The parameter $\mathcal{S}_{\rm eff}$ is related to $\mathcal{S}$ for $K^0_S\rho^0\gamma$ with a dilution factor $\mathcal{D} \equiv \mathcal{S}_{\rm eff}/\mathcal{S}_{K^0_S\rho^0\gamma}$ that depends on the $K^{*\pm}\pi^{\mp}$ components,

$$\mathcal{D} = \frac{\int[|F_A|^2 + 2\,{\rm Re}(F_A^* F_B) + F_B^*(\bar{K})F_B(K)]}{\int[|F_A|^2 + 2\,{\rm Re}(F_A^* F_B) + |F_B|^2]}, \quad (3)$$

where F_A, F_B are photon-helicity averaged amplitudes for $B^0 \to K^0_S\rho^0(\pi^+\pi^-)\gamma$ and $B^0 \to K^{*\pm}(K^0_S\pi^{\pm})\pi^{\mp}\gamma$, respectively. The factors $F_B(\bar{K})$, $F_B(K)$ distinguish between $K^{*-}\pi^+\gamma$ and $K^{*+}\pi^-\gamma$. The phase space integral is over the ρ^0 region.

The charged mode $B^+ \to K^+\pi^-\pi^+\gamma$ is first studied using a combination of various kaonic resonances with spin ≥ 1 to model the $K\pi\pi$ system. The amplitude for a kaonic resonance $K_{\rm res}$ that decays into particle c and subresonance r, where r later decays into particles a and b, can be modeled by the product of two Beit-Wigner functions:

$$M_{abc|r} = {\rm BW}(K_{\rm res}){\rm BW}(r)F_K(K_{\rm res})F_r f_{\rm spin}, \quad (4)$$

where BW is the relativistic Breit-Wigner line shape: ${\rm BW}(K_{\rm res}) = 1/(m^2_{K{\rm res}} - m^2_{abc} - im_{K{\rm res}}\Gamma_{K{\rm res}})$ and ${\rm BW}(r) = 1/(m_r^2 - m_{ab}^2 - im_r\Gamma_{ab})$. The width $\Gamma_{ab} = \Gamma_r(q/q_0)^{2L+1}(m_r/m_{ab})F_r^2$ is a function of q and q_0, the momenta of particle a in the r rest frame with mass m_{ab} and m_r, respectively. $F_K(K_{\rm res})$ and F_r are the Blatt-Weisskopf penetration factors [14] for resonances $K_{\rm res}$ and r. The spin factor $f_{\rm spin}$ for the resonances used in the nominal fit is $f_{\rm spin} = 1$ for $K_1^+(1270) \to K\rho^0$, $K^*\pi$, $K_1^+(1400) \to K^*\pi$ with a 1^+S wave; $f_{\rm spin} = \sin\theta$ for $K^*(1680) \to K\rho^0$, $K^*\pi$ with a 1^-P wave; $f_{\rm spin} = \sin\theta$ for $K_2^+(1430) \to K^*\pi$, $K\rho^0$ with a 2^+D wave. Here θ is the helicity angle of subresonance r.

Since every kaonic resonance decays to $K^*\pi$, we use events in a K^* region defined as $|m_{K^+\pi^-} - 0.896| < 0.075\ {\rm GeV}/c^2$ to study kaonic resonances in $B^+ \to K^+\pi^+\pi^-\gamma$. A two-dimensional (2D) $m_{K\pi}$, $m_{\pi\pi}$ fit is performed in the K^* region. In this fit, the yields for $q\bar{q}$ background are obtained from the $M_{\rm bc}$ fit. Other background parameters are obtained from MC calculations. In addition, the SCF component is further categorized depending on whether the K^+, π^- tracks are both correctly reconstructed.

Kaonic resonances with different spin-parity waves do not interfere if the decay plane orientation variables are integrated out. The 2D signal PDF in Eq. (4) is an incoherent sum of contributions from different spin parities with a phase space factor, after integrating out the $m_{K\pi\pi}$ variable. In the signal PDF, the yields of 1^+, 1^- kaonic resonances are obtained from a fit to the $m_{K\pi\pi}$ distribution in the K^* region. The rates for $K^+\rho^0$ relative to $K^{*0}\pi^+$ in decays of the $K^*(1680)$ and $K_2^*(1430)$ resonances are fixed according to the PDG values [12]. The phases for $K_{\rm res} \to K^{*0}\pi^+$ relative to $K_{\rm res} \to K^+\rho^0$ in the $K^*(1680)$, $K_2^*(1430)$ resonances are fixed to be -0.36 rad [15] and $-30°$ [16], respectively. The yields for the $K_2^*(1430)\gamma$ components are fixed based on [12]. The floating parameters are the rate and phase for $K_1(1270) \to K^*\pi$ relative to $K_1(1270) \to K\rho$.

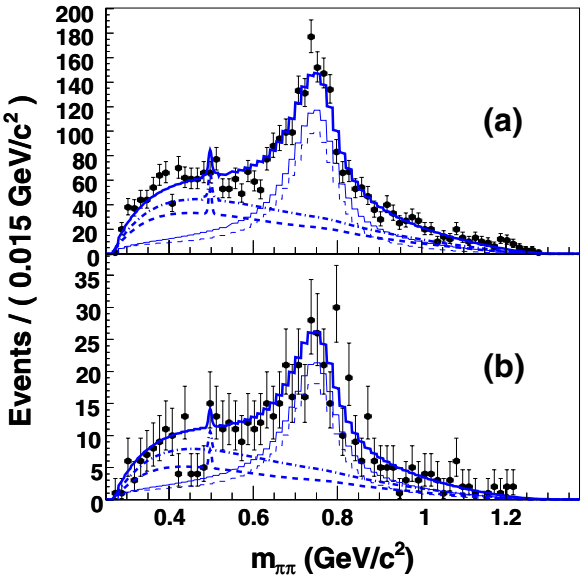

FIG. 3 (color online). $m_{\pi\pi}$ distributions for (a) $B^+ \to K^+\pi^-\pi^+\gamma$ and (b) $B^0 \to K^0_S\pi^+\pi^-\gamma$. The curves follow the convention in Fig. 1. The thin dashed curve is the correctly reconstructed $B \to K_1(1270)\gamma$ signal component.

The procedure is repeated for different fixed phases of $K_1(1400) \to K^*\pi$ relative to $K_1(1270) \to K\rho$, and we choose the one that gives the smallest χ^2. Figure 3 shows the distributions for $m_{\pi\pi}$ in the whole region without the K^* constraint, with $\chi^2/\mathrm{ndf} = 95/75$, where ndf denotes number of degrees of freedom, for 3(a) and $\chi^2/\mathrm{ndf} = 51/75$ for 3(b). The data distributions for $m_{K\pi\pi}$, $m_{K\pi}$, $m_{\pi\pi}$ in other regions also agree with our model.

Using isospin symmetry, we assume B^0 decay has the same parameters as B^+ for each kaonic resonance channel. We then obtain the contributions of the terms $|F_A|^2$, $|F_B|^2$ in Eq. (3), as listed in Table I.

Various systematic uncertainties in the dilution factor have been investigated. We added additional resonances $K_1(1270)[\to K\sigma, K^{*0}(1430)\pi, K\omega]\gamma$ and $K^*(1410)\gamma$ to the default model and repeated the fit procedure. Including $B \to K\sigma\gamma$ gives the largest systematic shift $\Delta\mathcal{D} = +0.17$. In this case, the σ has a C parity opposite to that of the ρ^0 and the dilution factor is $\mathcal{D} = \int[F_-(K)^*F_-(\bar{K}) - F_+^*F_+]/\int|F_- + F_+|^2$. Here F_+ is the photon-helicity averaged amplitude for $K_1(1270) \times (\to K^0_S\sigma)\gamma$, while $F_- = F_A + F_B$ [Eq. (3)]. In the absence of F_+, it reduces to Eq. (3). The next largest systematic shift $(+0.07)$ is from including $K_1(1270) \times [\to K^{*0}(1430)\pi]\gamma$. All other systematic errors are less than ± 0.02. The uncertainty from the assumption of isospin symmetry (± 0.01) is evaluated by floating kaonic resonance yields in a $m_{K^0_S\pi\pi}$ fit to $B^0 \to K^0_S\pi^+\pi^-\gamma$ events. Comparing to the $B^\pm$ results, the results are consistent with isospin symmetry, and the difference is taken as the uncertainty. The SCF uncertainty (± 0.01) is evaluated by using different signal MC models, and shifting the SCF fraction to zero, which is a conservative estimate for the multiple candidate effect. Other systematics include uncertainty in subresonance rates and phases, the mass and width of kaonic resonances, and statistical uncertainty from control sample data. Adding all the uncertainties in quadrature, we obtain $\mathcal{D} = 0.83^{+0.19}_{-0.03}$. By combining $\mathcal{S}_{\mathrm{eff}}$ and the dilution factor $\mathcal{D}$, we obtain $\mathcal{S}_{K^0_S\rho^0\gamma} = 0.11 \pm 0.33(\mathrm{stat})^{+0.05}_{-0.09}(\mathrm{syst})$.

TABLE I. The yields for each kaonic resonance and various interference terms in the final state $K^0_S\pi^+\pi^-\gamma$. Interf. denotes the interference between $K^0_S\rho^0\gamma$ and $K^{*+}\pi^-\gamma = 2\Re(F_A^*F_B)$.

	Total	$K^0_S\rho^0\gamma$	$K^{*+}\pi^-\gamma$	Interf.	$F_B^*(\bar{K})F_B(K)$
$K_{\mathrm{res}}(1^+)\gamma$	193.6	151.0	35.1	7.5	4.4
$[K_1^0(1270)\gamma]$	(167.6)	(151.0)	(38.0)	(−21.4)	(5.2)
$K_{\mathrm{res}}(1^-)\gamma$	24.2	11.3	8.0	4.9	1.3
$K_2^{*0}(1430)\gamma$	10.4	2.2	6.1	2.0	4.5
Sum	228.1	164.4	49.2	14.5	10.2

In summary, we have measured the time-dependent CP asymmetry in the decay $B^0 \to K^0_S\rho^0\gamma$ using events with $m_{K\pi\pi} < 1.8\ \mathrm{GeV}/c^2$ and $0.6 < m_{\pi\pi} < 0.9\ \mathrm{GeV}/c^2$. We obtain the CP-violating parameters $\mathcal{S}_{K^0_S\rho^0\gamma} = 0.11 \pm 0.33(\mathrm{stat})^{+0.05}_{-0.09}(\mathrm{syst})$ and $\mathcal{A}_{\mathrm{eff}} = 0.05 \pm 0.18(\mathrm{stat}) \pm 0.06(\mathrm{syst})$. With the present statistics, the result is consistent with zero and comparable in precision to the measurement in $B^0 \to K^0_S\pi^0\gamma$ [4,5]. This is the first measurement of CP asymmetry parameters in the $B^0 \to K^0_S\rho^0\gamma$ mode.

We thank the KEKB group for excellent operation of the accelerator, the KEK cryogenics group for efficient solenoid operations, and the KEK computer group and the NII for valuable computing and SINET3 network support. We acknowledge support from MEXT and JSPS (Japan); ARC and DEST (Australia); NSFC (China); DST (India); MOEHRD, KOSEF and KRF (Korea); KBN (Poland); MES and RFAAE (Russia); ARRS (Slovenia); SNSF (Switzerland); NSC and MOE (Taiwan); and DOE (U.S.A.).

[1] D. Atwood, M. Gronau, and A. Soni, Phys. Rev. Lett. **79**, 185 (1997).
[2] T. Gershon and A. Soni, J. Phys. G **34**, 479 (2007).
[3] D. Atwood, T. Gershon, M. Hazumi, and A. Soni, Phys. Rev. D **71**, 076003 (2005).
[4] Y. Ushiroda *et al.* (Belle Collaboration), Phys. Rev. D **74**, 111104 (2006).
[5] B. Aubert *et al.* (*BABAR* Collaboration), arXiv:0708.1614.
[6] A. Abashian *et al.* (Belle Collaboration), Nucl. Instrum. Methods Phys. Res., Sect. A **479**, 117 (2002).
[7] S. Kurokawa and E. Kikutani, Nucl. Instrum. Methods Phys. Res., Sect. A **499**, 1 (2003), and other papers included in this volume.

[8] P. Koppenburg *et al.* (Belle Collaboration), Phys. Rev. Lett. **93**, 061803 (2004).
[9] K. F. Chen *et al.* (Belle Collaboration), Phys. Rev. Lett. **98**, 031802 (2007).
[10] S. H. Lee *et al.* (Belle Collaboration), Phys. Rev. Lett. **91**, 261801 (2003).
[11] Y. Ushiroda *et al.* (Belle Collaboration), Phys. Rev. Lett. **100**, 021602 (2008).
[12] W. M. Yao *et al.* (Particle Data Group), J. Phys. G **33**, 1 (2006).
[13] T. Skwarnicki, Ph.D. thesis, Institute for Nuclear Physics, Krakow, 1986; DESY Internal Report No. DESY F31-86-02, 1986. The function is widely used to describe asymmetric distributions caused by shower leakage in crystal calorimeters.
[14] J. Blatt and V. Weisskopf, *Theoretical Nuclear Physics* (John Wiley & Sons, New York, 1952). The penetration factor is defined as 1 for S wave, $\frac{\sqrt{R^2p^2}}{\sqrt{1+R^2p^2}}$ for P wave, and $\sqrt{\frac{(Rp)^4}{(Rp)^4+3(Rp)^2+9}}$ for D wave, where p denotes the momentum of the daughter particle in the rest frame of the mother particle. We choose the radius to be $R = 0.3$ fm
[15] D. Aston *et al.*, Nucl. Phys. **B292**, 693 (1987).
[16] C. Daum *et al.* (ACCMOR Collaboration), Nucl. Phys. **B187**, 1 (1981).